Materials Advances

ROYAL SOCIETY OF CHEMISTRY

PAPER

View Article Online
View Journal | View Issue

Cite this: *Mater. Adv.*, 2023, 4, 3593

Fluorine-free synthesized tantalum carbide (Ta_2C Mxene) as an efficient electrocatalyst for water reduction and nitro compound reduction†

Aathilingam Vijayaprabhakaran[ab] and Murugavel Kathiresan *[ab]

One of the eco-sustainable sustainable ways to generate hydrogen, which is considered a clean energy source, involves the electrochemical process. On the other hand, identifying the most effective heterogeneous catalyst is crucial for amine synthesis from nitro compounds in order to determine the optimum catalytic activity, stability, and reusability. Herein, we report the preparation of a 2D tantalum carbide MXene *via* the fluorine-free etching method and its application in catalysis (nitro reduction) and electrocatalysis (HER and nitro reduction). It is well-known that due to their layered structure, MXenes show better catalytic activities, and hence they find applications in catalysis. Ta_2AlC (MAX phase) and Ta_2C (MXene) were evaluated for their electrocatalytic activity in the hydrogen evolution reaction. The electrocatalyst Ta_2C MXene exhibited overpotentials of 223 mV to reach 10 mA cm^{-2} current density when tested under standard HER conditions (0.5 M H_2SO_4), and furthermore, the electrocatalytic reduction behavior of Ta_2C MXene towards the electrochemical reduction of 4-NP was tested in 1 M KOH. Galvanostatic electrolysis was performed in a divided cell using Ta_2C modified carbon cloth as the cathode, and Pt as the anode separated by a Nafion membrane, and it showed 72% product conversion and 96% faradaic efficiency. The progress of the galvanostatic electrolysis was monitored using *ex situ* Raman and UV-Vis spectroscopy. Similarly, the reducing behavior of Ta_2C towards the reduction of 4-nitrophenol to 4-aminophenol in the presence of $NaBH_4$ was tested. The Ta_2C MXene displayed improved catalytic activity with pseudo-first-order kinetics. Ta_2C nanoparticles completely reduced all three nitro compounds (10 mL each), 4-NP (216 μM–17 min), 2,4-dinitrophenol DNP (163 μM–25 min) and 2,4,6-trinitrophenol TNP (131 μM–36 min). Furthermore, in all these studies, the Ta_2C MXene exhibited improved catalytic performance and stability.

Received 9th May 2023,
Accepted 12th July 2023

DOI: 10.1039/d3ma00223c

rsc.li/materials-advances

1. Introduction

Hydrogen is one of the essential chemical feedstocks of future energy applications,[1] and it can also be utilized to hydrogenate a variety of organic molecules. The major downside of these processes has been their high cost and low energy efficiency in generating low-purity hydrogen over the years.[2] It is generally known that platinum displays superior electrocatalytic activity for the HER in an acidic solution at near-zero potentials; it displays 20 mV at 1 mA cm^{-1} and is regarded as the most efficient catalyst.[3,4] Unfortunately, the cost, availability, and sustainability of such platinum-based catalysts for future hydrogen production are onerous.[5] Hence, the development of active electrocatalysts based on non-noble metals with less overpotential for the hydrogen evolution reaction becomes essential to improve the process efficiency.[6,7] Hydrogen is also used in the reduction of several organic compounds, such as hazardous 4-nitrophenol (4-NP), an environmental pollutant,[8] particularly a major contaminant of water resources.[9] Among them, organic wastewater containing 4-nitrophenol has a number of major issues,[10,11] including a protracted period of pollution, a huge amount of discharge, substantial damage, a high level of toxicity, and a treatment process that is incredibly challenging. 4-Aminophenol is the main intermediate for paracetamol, and major commodity chemicals (acebutolol, ambroxol, and sorafenib) used extensively in the production of pharmaceuticals, dyes, and polymers. Moreover, the green reduction of the highly pollutant 4-nitrophenol has great significance in the industrial production of 4-aminophenol.[12,13] Nevertheless, the majority of approaches merely collect harmful substances and necessitate additional calcination treatment, like adsorption, to effectively eradicate 4-NP. As compared to other techniques, catalytic

[a] *Academy of Scientific and Innovative Research (AcSIR), Ghaziabad 201002, India*
[b] *Electro Organic and Materials Electrochemistry Division, CSIR-CECRI, Karaikudi, 630003, Tamil Nadu, India. E-mail: kathiresan@cecri.res.in*

† Electronic supplementary information (ESI) available. See DOI: https://doi.org/10.1039/d3ma00223c

hydrogenation is the most eco-friendly, effective, and feasible way to convert 4-NP to 4-AP. The reaction could be performed in water using a hydrogen source such as $NaBH_4$, which is considered a green route for this reduction reaction.[14,15]

MXenes are a new type of material discovered a decade ago (in 2011);[16] which contain transition metal carbides, nitrides, and carbonitrides, and they emerged as a new class of two-dimensional materials.[17,18] MXenes are synthesized *via* a selective etching process to disperse the layers from stacks, generally using a solution of HF, KF or LiF, or HCl that have high toxicity/corrosiveness.[19,20] Various etching methods have been developed for preparing MXene sheets,[21] but the alkali etching method increases the material's performance and is ecologically better compared to the fluoride etching method to remove aluminium from the MAX phase in an efficient way.[22,23] In general, the catalytic applications of MXenes rely on the nature of the transition metals and the terminal groups.[24] Transition metal carbides show higher catalytic activities for the reduction of nitro compounds.[25] Recently, Zhang *et al.* reported the synthesis of $Ti_3C_2T_x$ (T = OH, O) using the alkali-assisted hydrothermal technique that was based on the Bayer process to purify bauxite. Using this approach, the Ti_3C_2 MXene was synthesized with 92% purity.[26] Kuznetsov *et al.* reported the preparation of Co:Mo_2CT_x MXene and its application in the HER which displayed a low overpotential of 250 mV at a current density of 10 mA cm^{-2} in 1N H_2SO_4 solution.[27] Pumera and co-workers reported the HER application of Mo_2TiAlC_2 max phase which showed a low overpotential of 570 mV in 0.5 M H_2SO_4.[28] Later, the photoelectrochemical HER activity of the fluorine-doped Ta_2AlC max phase was reported by the same group, wherein the Ta_2AlC displayed an overpotential of 786 mV at 10 mA cm^{-2} current density.[29] Le *et al.* prepared nitrogen-doped $Ti_3C_2T_x$ by annealing the sample at 600 °C and the heat treated sample displayed superior HER activity (overpotential of 198 mV at 10 mA cm^{-2}) compared to pristine $Ti_3C_2T_x$.[30] Very recently, Tang *et al.* reported the preparation of mesoporous nitrogen-doped carbon layer coupled MoC nanodots and 2D Ti_3C_2 MXene composites and evaluated their electrocatalytic properties towards the HER in 0.5 M H_2SO_4.[31] The composites displayed a low overpotential of 159 mV at 10 mA cm^{-2} current density. Rasheed *et al.* reported the catalytic activity of $Nb_4C_3T_x$@PdNP MXene composites towards the reduction of 4-nitrophenol and organic dyes.[32] About 200 μL of 0.5 mg mL^{-1} $Nb_4C_3T_x$@PdNP catalyst was added to 400 μL of 1 mM 4-NP in the presence of $NaBH_4$, which reduced 4-NP within 3 min and the catalyst was reused for up to 5 consecutive cycles without much loss in the catalytic activity. Chen *et al.* prepared CQD@Ag/Ti_3C_2 MXene composites and used them to catalyse the reduction of 4-NP.[25] Recently, Zhao *et al.* reported the use of Ag/Ni-MOF on Ni foam as the cathode for the electrochemical reduction of 4-nitrophenol, and exceptional conversion and faradaic efficiency of 98.4% and 99.8% were achieved.[33]

The present study reports alkali-assisted hydrothermal synthesis of Ta_2C MXenes, which are also known as fluorine-free MXenes. The as-synthesized MXene was thoroughly characterized and tested for its electrocatalytic activity in the hydrogen evolution reaction, and in the electrochemical and chemical reduction of substituted 4-nitrophenol analogs.

2. Materials and methods

2.1 Materials

Ta_2AlC MAX Phase (nano research elements-Haryana), KOH, LiCl, ethanol, sulfuric acid, 4-nitrophenol (4-NP), 2,4-dinitrophenol (DNP), and 2,4,6-trinitrophenol (TNP) were of analytical grade and used without further purification (Sigma-Aldrich Pvt Ltd), and the water utilized in this experiment was double distilled over alkaline potassium permanganate.

2.2 Synthesis of Ta_2C MXenes

4.5 g of potassium hydroxide pellets were dissolved into a minimum amount of deionised water to make a concentrate base solution; then 1.5 g of Ta_2AlC powder was added, mixed with the base solution, and stirred for 5 minutes. This mixture was transferred into a stainless steel 50 mL autoclave containing a Teflon vessel, sealed and heated to 150 °C for 24 h. After which, the obtained product was centrifuged and washed with deionised water to reach pH 7.[34] The etched Ta_2C MXene (Ta_2C-B) (B stands for bulk) sediment was then dispersed in a 0.5 M LiCl solution, stirred at room temperature for 5 hours, then filtered and washed with deionised water *via* centrifugation.[35] Finally, the sample was mixed with 50 mL of ethanol and then ultrasonicated for 10 hours. Then, the sample was centrifuged, and dried in a vacuum oven at 80 °C for 12 h. The schematic synthesis process is shown in Fig. 1.[36] Then the prepared MXene (Ta_2C-E) (E stands for exfoliated) was subjected to characterization to confirm its chemical integrity, functionalities, and morphology.

3. Results and discussion

3.1 Characterization

A comparison of the Raman spectra of the MAX phase and the tantalum carbide MXene confirms the removal of aluminium from the MAX Phase as shown in Fig. 2(a). A_1g (ω2, ω3) and E_1g ω5 are Raman active modes of Ta_2C-E layers; E_2g (ω1, ω4) are attributed to Ta_2AlC layers as per previous reports.[37,38] The vibration involving Al, *i.e.*, E_2g (ω1, ω4) is suppressed in Ta_2C-E due to the absence of aluminium or exchange of Al with lower atoms because of basic etching. This confirms the complete etching of Al from the MAX phase. The vibrational modes of ω5 were weak in comparison with tantalum aluminium carbide and merged, thereby providing the information that the tantalum carbide was still in the closely packed structure after the removal of Al and the probe sonication. The X-ray diffraction (XRD) patterns confirm the successful formation of Ta_2C-E MXene. The diffraction peaks of Ta_2C-E (JCPDS: 96-210-3619) are analogous to Ta_2O planes 011, 020, 021, 121, 022, and 122 ascribed to 2θ = 31.7, 45.4, 51.1, 56.4, 66.2, and 70.8 and different from that of the Ta_2AlC MAX phase (JCPDS: 00-029-0092); 100, 101, and 103 planes corresponding to 2θ = 28.3, 29.4, and 37.1 were suppressed.[39,40] The peak intensities clearly indicate the elimination of aluminium from the starting material (Fig. 2(b)). The MAX phase was initially present in a hexagonal structure but after etching it was transformed into a cubic

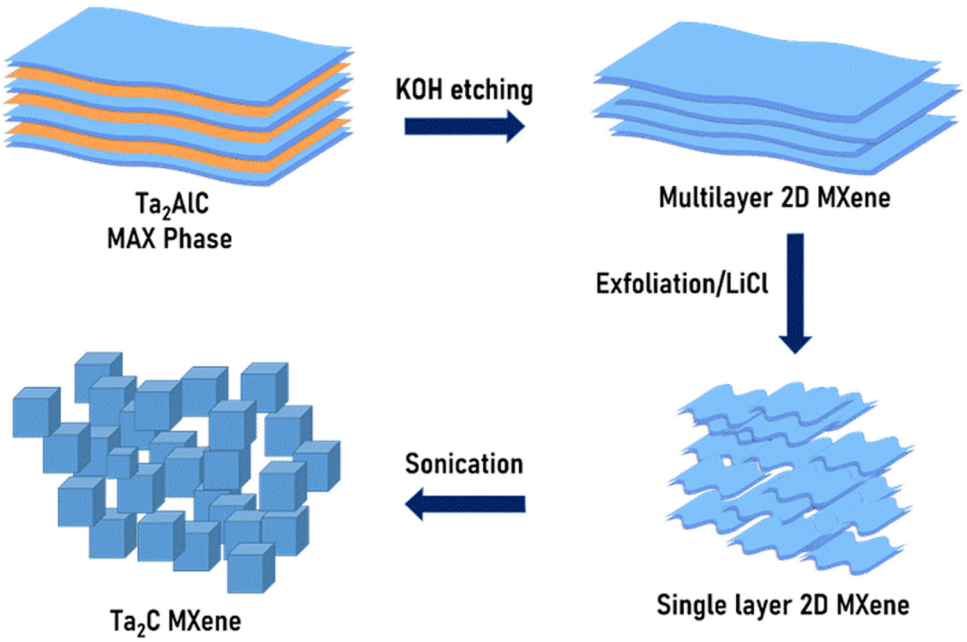

Fig. 1 Schematic alkali etching process for the Ta_2AlC MAX phase.

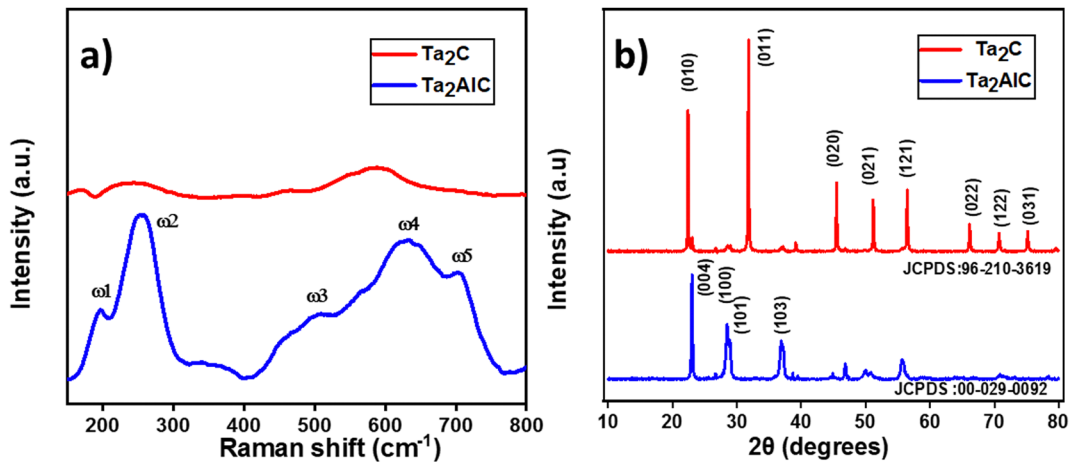

Fig. 2 (a) Raman spectra of the Ta_2AlC MAX phase and Ta_2C-E (b) XRD patterns of Ta_2AlC and Ta_2C-E.

nanomaterial.[41] Energy Dispersive X-ray spectroscopy (EDS) results confirm the complete removal of aluminium by the etching process. The expected elements presented after etching show some amount of potassium (7.5%) and an increased amount of oxygen in the etched materials which indicates that the oxidation of nanomaterials is unavoidable (Fig. S1, ESI†).

The morphology of Ta_2AlC and Ta_2C-E was analyzed using a scanning electron microscope, which reveals the microstructure of the multilayered MAX phase, and in the case of etched materials (Ta_2C-B), the sheets are slightly expanded due to the removal of aluminium (Fig. 3(a)–(c)). Furthermore, the dispersion is confirmed by the addition of $LiCl_2$. In the FESEM image given in Fig. 3(d), the etched sample appears like a cubic aggregate.

To obtain further morphological insights HR-TEM analysis was performed (Fig. 4(a) and (b)) which reveals a cube like structure of Ta_2C-E. The very crystalline nature is evident from the selected area electron diffraction patterns given in Fig. 4(c). The HAADF (high angle angular dark field) elemental mapping results shown in Fig. 4 confirm the equal distribution of Ta and C in Ta_2C-E.

Besides, XPS spectra was recorded to understand the details of the chemical composition of Ta_2AlC and Ta_2C-E. Fig. S2(a) and (b) (ESI†) show the XPS survey spectrum. The absence of the Al peak in the Ta_2C-E MXene confirms the complete etching of Al and the presence of remaining elements. The deconvoluted spectrum of Ta 4f shows peaks (Fig. S3(d), ESI†) at 24.2 and 26.0 eV, related to the Ta $4f_{7/2}$ and $4f_{5/2}$ matching with the

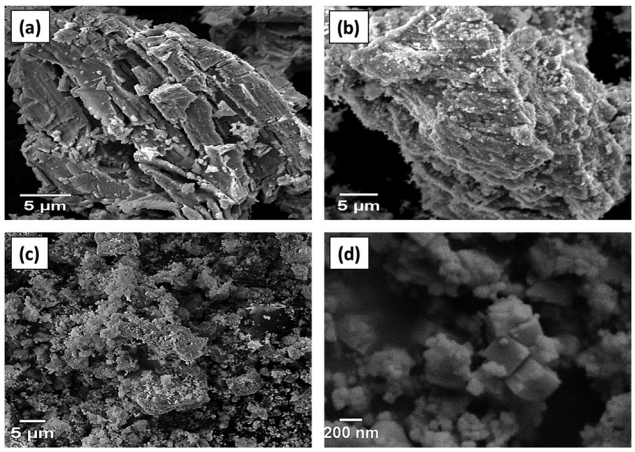

Fig. 3 SEM micrograph images of (a) MAX phase, (b) after alkali etching of Ta_2C-B, (c) Ta_2C-E, and (d) FESEM image of Ta_2C-E MXene.

Ta–C bond and it was evident that Ta exists as Ta^{4+} in Ta_2C MXene. A comparison of the deconvoluted C 1s XPS spectra of the MAX phase and MXene confirms the appearance of new carbon peaks at ≈290 eV and ≈292 eV, an indication for the removal of aluminium (Fig. S3(e), ESI†).

3.2 Electrocatalytic activity

(a) HER investigations. The electrocatalytic activities of Ta_2C MXene and its MAX phase (Ta_2AlC) were evaluated by obtaining linear sweep voltammetry (LSV), cyclic voltammetry (CV) and chronoamperometry data in acidic medium (0.5 M H_2SO_4) under standard HER conditions (Fig. 5(a) and (b)). Initially, cyclic voltammetry curves (CVs) were recorded for both the samples for 1000 cycles at a scan rate of 100 mV s^{-1}, after which linear sweep voltammograms (LSVs) were recorded at a 2 mV s^{-1} scan rate. A typical polarization curve demonstrates that the modified Ta_2C electrode displayed a low over potential and the other electrocatalyst showed a higher over potential. It is evident that among the prepared electrocatalysts, Ta_2C-E MXene exhibited the lowest overpotential of 223 mV to reach 10 mA cm^{-2} current density and Ta_2C-E showed a higher current density of 358 mA cm^{-2} compared to other electrocatalysts indicating its excellent HER performance. The benchmark catalyst Pt–C exhibited 77 mV to reach 10 mA cm^{-2} under similar conditions. Furthermore, the Tafel slope was plotted by taking a log of the current density and the overpotential to understand the HER kinetics (Fig. 5(d)). The Tafel values obtained for the electrocatalysts were, MAX phase – 159 mV dec^{-1}, alkali etched sample Ta_2C-B – 132 mV dec^{-1}, Ta_2C-E MXene – 75 mV dec^{-1}, and Pt-C – 44 mV dec^{-1}. It is apparent that the Ta_2C MXene showed the lowest Tafel slope value next to the Pt–C, indicating its facile OER kinetics, while the other samples such as the MAX phase and alkali etched samples displayed higher Tafel slope values. EIS (Electrochemical impedance spectroscopy) investigations were carried out in the range of 0.05 Hz to 10^6 Hz. It is obvious that the Ta_2C-E (305.5 Ω) MXene displayed very low R_{ct} compared to the MAX phase (Fig. 5(c)), indicative of the low ion transport resistance of Ta_2C-E MXene. Another crucial aspect to consider when evaluating the effectiveness of catalysts is their stability under investigated conditions using chronoamperometric analysis. The chronoamperometric analysis of Ta_2C-E MXene under HER conditions revealed the excellent stability of the catalyst over 24 h without any degradation in its catalytic activity (Fig. 5(e)). The lower onset potential and higher cathodic peak current were observed for Ta_2C-E in 0.5 M H_2SO_4 medium, indicating its superior electrocatalytic activity under these conditions, and the catalyst Ta_2C-E was durable over 24 h under the tested conditions.[28,29,42] The HER activity comparison table of identical electrocatalysts is shown in Table S1 (ESI†) which shows that Ta_2C-E MXene performs better even without compositing. After the HER stability test, we found no differences in the

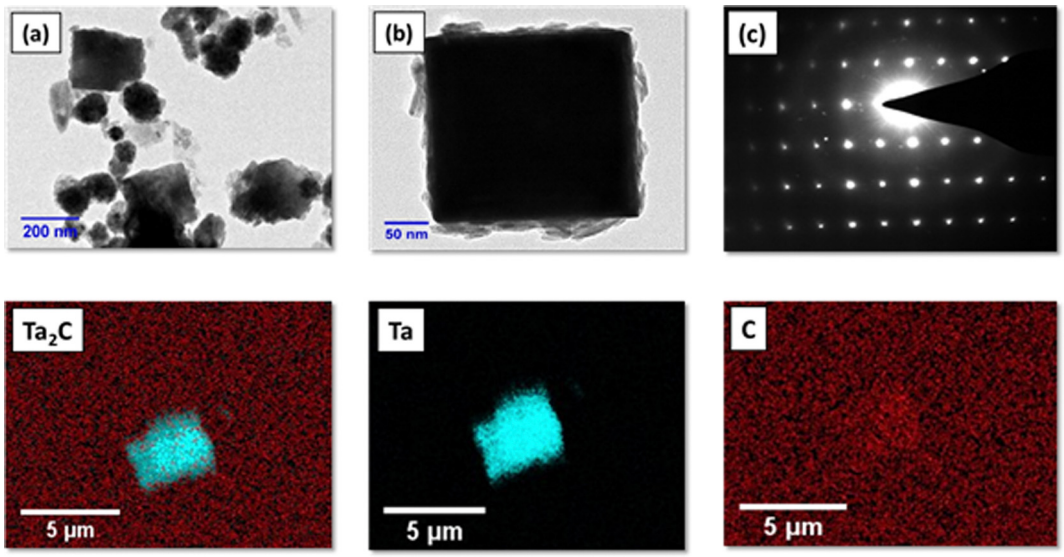

Fig. 4 HR-TEM images of Ta_2C-E (a) and (b) and (c) selected area electron diffraction (SAED) image and HAADF mapping image of Ta_2C-E, Ta, and C.

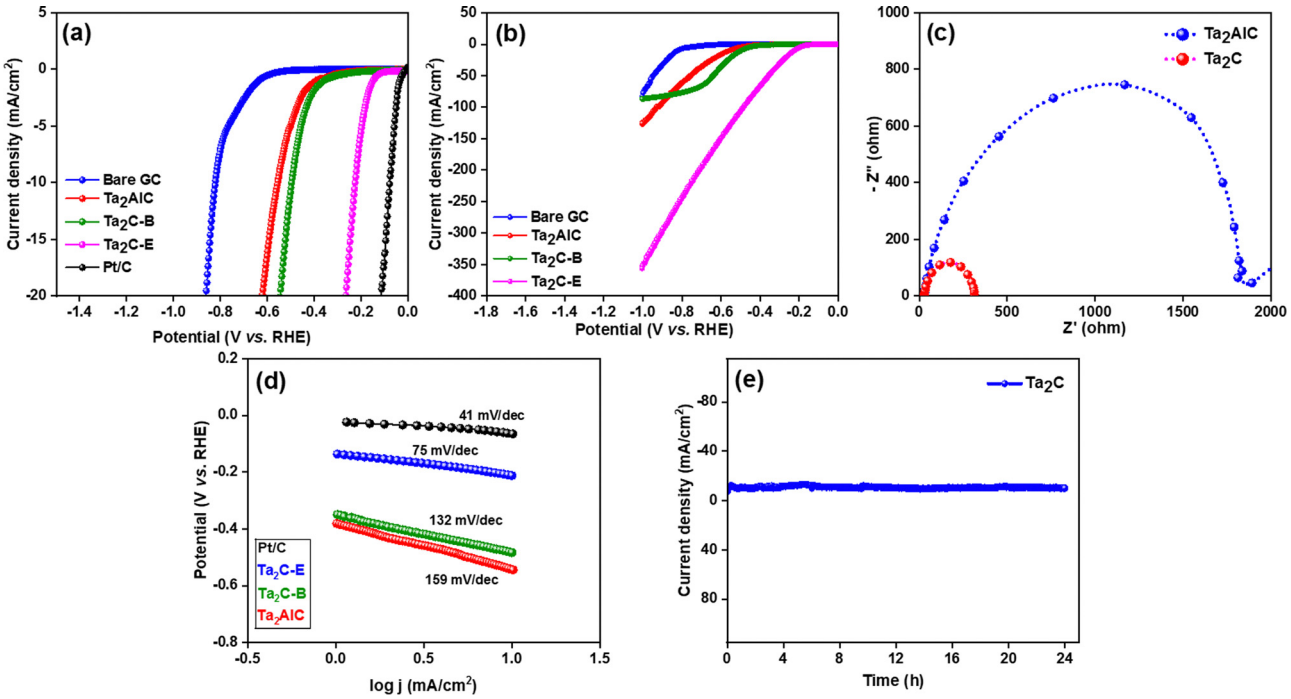

Fig. 5 (a) LSV studies on bare glassy carbon (GC) electrode, modified GC, GC/Ta_2AlC, GC/alkali etched Ta_2AlC-B and GC/Ta_2C-E in 0.5 M H_2SO_4/H_2O at a 2 mV s^{-1} scan rate, (b) LSV at the maximum current range, (c) EIS spectrum of Ta_2AlC and Ta_2C-E, (d) Tafel slopes of Ta_2AlC and Ta_2C-E modified electrodes, and (e) a stability study of GC/Ta_2C-E over a duration of 24 h.

morphology, indicating the catalysts' outstanding reliability under HER circumstances (Fig S4, ESI†).

(b) Electrochemical conversion of 4-nitrophenol to 4-aminophenol. The electrochemical conversion of 4-nitrophenol to 4-aminophenol has great importance from an industrial perspective as 4-NP is a common organic pollutant.[43] Although there are chemical methods that efficiently convert 4-NP to 4-AP, an important intermediate for dyes and drugs, these methods produce secondary pollutants in the form of sludge, or they utilize expensive noble metal-based catalysts. In an electrochemical method, 4-NP is converted to 4-AP in a more eco-friendly way, where the electro-catalyst initiates the reduction process in aqueous medium which also acts as a hydrogen source.[33,44] In this work, we have evaluated the electrocatalytic performance of Ta_2C-E MXene towards the reduction of 4-NP to 4-AP in 1 M KOH medium. Initially, linear sweep voltammograms were obtained in the presence of 4-nitrophenol (10 mM) using 1 M KOH as an electrolyte.[45,46] Fig. 6(a) shows the LSV response of Ta_2C-E MXene with and without 4-NP and Fig. 6(b) shows the LSV response of bare, MAX phase and Ta_2C MXene in the presence of 4-NP. It is evident that in the absence of 4-NP, no reduction peak could be observed. In the presence of 4-NP, an onset potential of −0.27 V was noted for the reduction of 4-NP and the reduction potential of 4-NP was approx. −0.9 V with a current density of −14 mA cm^{-2}. Furthermore, the comparative LSV shows that Ta_2C-E exhibits better electrocatalytic activity than the bare and MAX phase which is evident from their current density as well as onset potentials. Fig. 6(c) shows the EIS spectra of the bare, MAX phase and Ta_2C-E samples, showing a lower R_{ct} value for Ta_2C-E. Also, Fig. S5(e) (ESI†) shows a comparison of EIS with and without 4-NP, and it is evident that in the presence of 4-NP, Ta_2C-E displayed a lower R_{ct} value indicating a facile reduction process. The Tafel slope was calculated from the corresponding LSV data and given in Fig. 6(d), and it is evident that Ta_2C-E exhibited a lower Tafel slope value of 128 mV dec^{-1} indicative of better nitrophenol reduction kinetics than its MAX phase.[33] Fig. S5(f) (ESI†) compares the Tafel values of Ta_2C-E in the absence and presence of 4-NP. It can be manifested that in the presence of 4-NP, Ta_2C-E displays the lowest Tafel slope value (123 mV dec^{-1}).

The electrochemical reduction of 4-NP follows three consecutive two electron reduction pathways. In the first step, 4-NP is reduced to 4-nitrosophenol by 2 electron 2 proton transfer. In the second subsequent step, 4-nitrosophenol is reduced to 4-hydroxylaminophenol by 2 electron, 2 proton transfer. Finally, in the third step, 4-hydroxylaminophenol is converted to 4-aminophenol by another 2 electron, 2 proton transfer. It is noteworthy that in each step, 2 electron and 2 protons are utilized. After LSV investigations, galvanostatic electrolysis of 4-nitrophenol was performed in a divided cell set up using Ta_2C-E coated carbon cloth electrode (1 × 1 cm) as the cathode and Pt sheet as the anode, separated by a Nafion membrane at current densities of 40, 80, 120, 160 and 200 mA cm^{-2} at room temperature [the divided cell set up is essential to prevent the anodic polymerization of 4-aminophenol]. At the end of electrolysis, the reaction mixture was worked up and the products were confirmed using H^1 and C^{13} NMR spectroscopy (Fig. S7(a) and (b), ESI†). From Fig. 7, it can be realized that a better yield

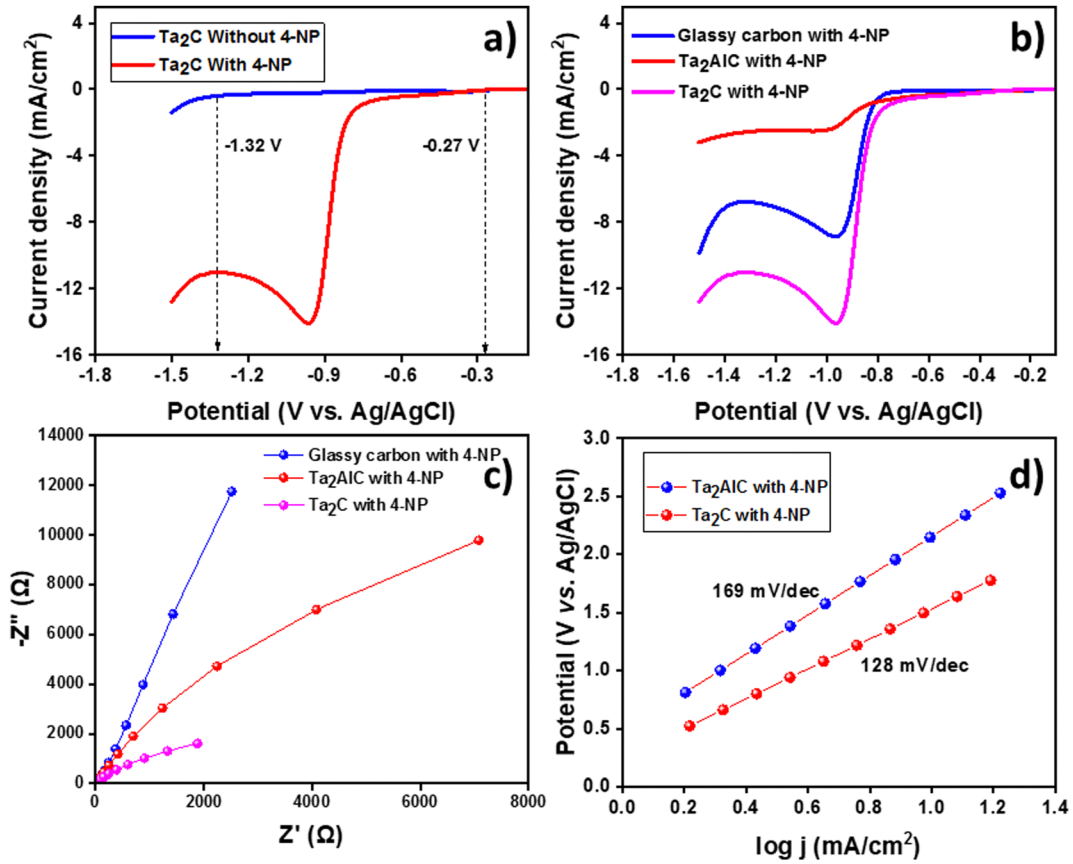

Fig. 6 (a) LSV studies with and without 4-NP on modified Ta_2C-E (1 M KOH/H_2O at 50 mV s^{-1} scan rate), (b) LSV at the maximum current range compared to the bare and MAX phase, (c) EIS spectrum of Ta_2AlC and Ta_2C-E and (d) Tafel slopes of Ta_2AlC and Ta_2C-E with 4-NP.

was obtained when the current density was 160 mA cm^{-2}, however with an increase in current density, a decrease in faradaic efficiency is noted.

The progress of the electrocatalytic reduction of 4-NP to 4-AP in 1 M KOH electrolyte was monitored using *ex situ* Raman and UV-Vis spectroscopy.[47] Fig. 8(a) shows the Raman spectra of 4-nitrophenol, where the predominant peaks such as C–H ip bending (1116, 1172, and 1292 cm^{-1}), NO_2 symmetric stretching (1339 cm^{-1}) and NO_2 bending (858 cm^{-1}) were observed.[48] The decrease in Raman intensity of the NO_2 symmetric stretch

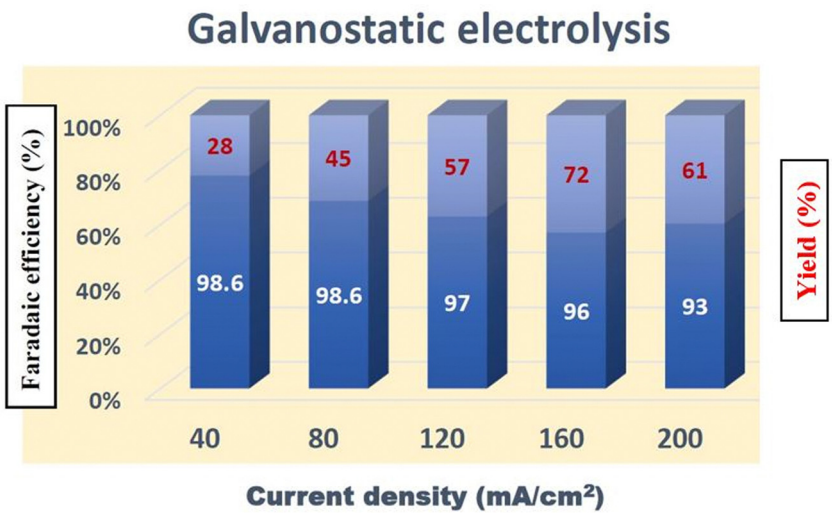

Fig. 7 Results of the galvanostatic electrolysis of 4-nitrophenol to 4-aminophenol at different current densities (faradaic efficiency is given in dark blue shades with FE indicated in white color and yield% is given in light blue shades with the corresponding yield indicated in red color).

at 1292 cm^{-1} is monitored with respect to reaction time, as this is a key indicator for the disappearance of the nitro peak. It can be observed from Fig. 8(a) that a rapid decrease in the Raman intensity is observed until 150 min, after which the peak completely disappeared indicating the successful conversion of 4-NP to 4-AP by galvanostatic electrolysis. Furthermore Fig. 8(c) shows the presence of NH_2 wagging (848 cm^{-1}) and NH_2 twisting (1172 cm^{-1}) peaks on both commercial and electrochemically synthesized samples confirming the successful formation 4-AP. The kinetics of the catalytic process was found to be pseudo-first order reaction as shown in Fig. 8(b). As already mentioned, the *ex situ* Raman measurements enabled us to observe the reaction's changes on a preparative scale. Generally electrolysis is a very slow process so that assignment of the observed Raman bands is performed on the basis of previously reported data. UV-Vis spectroscopy is a widely used and standardized approach, that is frequently employed to monitor the progress of the conversion of 4-NP to 4-AP. The large absorption cross section of 4-NP prevents UV-Vis spectroscopy from being able to monitor the process under our synthetic circumstances and volume and catalyst concentration are the major reasons for the rate constant differences. Also, the galvanostatic electrolysis was carried out in pH 11–12 and catalytic investigations were carried out in aqueous medium at neutral pH. The conversion of 4-NP to 4-AP was also monitored by recording UV-Vis spectroscopy every 30 min and the plot is shown in Fig. 8(d). The kinetics of the reaction was found to be pseudo-first order reaction (Fig. S6, ESI†) and the slope of $\ln(A_0/A_t)$ *vs.* time, where A_0 and A are the absorbances (λ_{max} = 402 nm) at time t_0 and t, respectively, is therefore regarded to be the apparent reaction rate constants (k_{app}) similar to the rate constant calculated at 1292 cm^{-1} in Raman spectroscopy.

3.3 Chemical reduction of 4-nitrophenol

The catalytic reduction of hazardous nitrophenol to the corresponding aminophenol derivatives by surplus sodium borohydride in the presence of the catalyst (MXene and MAX phase) was selected as a model test reaction to assess the catalytic performance of Ta_2C-E MXene and the progress of the reduction was monitored by UV-Vis spectroscopy. 4-Nitrophenol shows an absorption maxima at 400.8 nm and upon reduction, 4-aminophenol is formed, which shows an absorption maximum at 298.6 nm. Typically, either of these two peaks is examined to monitor the reduction process, *i.e.*, when reduction occurs, a decrease in peak intensity at 400.8 nm with respect to time was noted, and complete disappearance of this peak indicates completion of the reduction process or increase in the intensity of the peak at 298.6 nm with respect to time is monitored. The reduction of nitrophenol in the presence of the

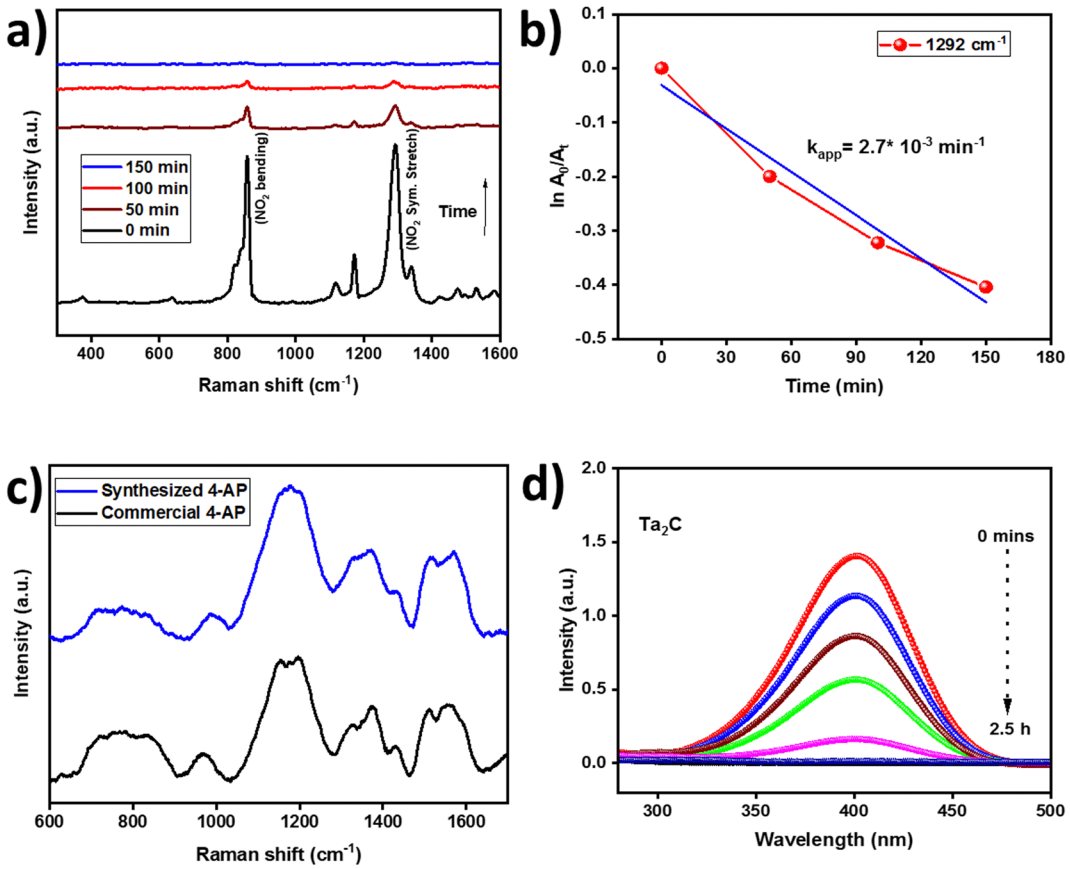

Fig. 8 (a) *Ex situ* Raman spectra of an electrolytic mixture containing 4-NP = 0.3 g (270 mM), in 1 M KOH, T = 25 °C. (b) Kinetic study of the Raman intensity at 1292 cm^{-1} during the electrocatalytic reduction of 4-NP. (c) Raman scattering spectra of commercial 4-NP and electrolyzed sample at t = 150 min, and (d) UV-Vis absorption spectra revealing the reduction process.

catalyst and $NaBH_4$ initially leads to the formation of nitrophenolate ion which is then reduced to aminophenolate [initially in the presence of sodium borohydride the solution was light yellow; after the addition of $NaBH_4$ a small amount of bubbles were observed due to the reaction between $NaBH_4$ and water; then, followed by the addition of catalyst, a large amount of bubbles was observed, and finally the solution turned colourless].[49] To cross-check the role of catalyst in the reduction of nitrophenols, a blank reaction was run with 4-nitrophenol without the catalyst in the presence of excess $NaBH_4$. No reduction was observed. The catalytic activity of the as-synthesized Ta_2C-E MXene was tested towards the reduction of 4-nitrophenol using surplus $NaBH_4$ in an aqueous medium at RT, and the results were compared with its MAX phase as given in Fig. 9(a) and (b). It is observed that the MAX phase took about 90 min for the reduction of 10 mL of 4-nitrophenol (216 μM) with 1 mg of MAX phase catalyst, however the Ta_2C catalyst took only 17 min to reduce the same under identical concentrations, revealing its superior catalytic performance in the reduction of hazardous 4-nitrophenol. Different volumes of 4-nitrophenol (216 μM) were reduced under identical conditions, and the results indicate that they were reduced at different time intervals shown in Fig. S9(d)–(f) (ESI†), however, the time interval trend followed a linear relationship with respect to concentration.[50] Furthermore, the catalyst was checked for its reusability, five consecutive catalytic cycles were performed using 5 mL of 4-nitrophenol (216 μM) with 1 mg of Ta_2C-E catalyst and the results are provided in Fig. S8 (ESI†); it is noted that after each repeated cycle, a slight decrease in the efficiency (1% decrease) was noted.

It is evident that Ta_2C shows excellent catalytic performance towards the reduction of 4-nitrophenol in the presence of excess $NaBH_4$ under aqueous conditions. To further extend the scope of Ta_2C based reduction catalysis, the reduction of other hazardous nitro compounds such as 2,4-dinitrophenol (DNP) and 2,4,6-trinitrophenol (TNP) was also tested under similar conditions.[51] DNP and TNP show absorption maxima at 352.6 and 389.6 nm, respectively. Upon reduction, the corresponding aminophenol peaks were observed at 299.04 and 301.2 nm, respectively (Fig. 9(c) and (d)). It is apparent that the Ta_2C catalyst took 25 and 36 min to reduce DNP (163 μM) and TNP (131 μM) respectively. From the results, it can be concluded that Ta_2C-E shows excellent catalytic activity towards the reduction of hazardous nitrophenols to aminophenols.

Table 1 compares the performance of various 2D layered materials towards the reduction of 4-nitrophenol in the presence

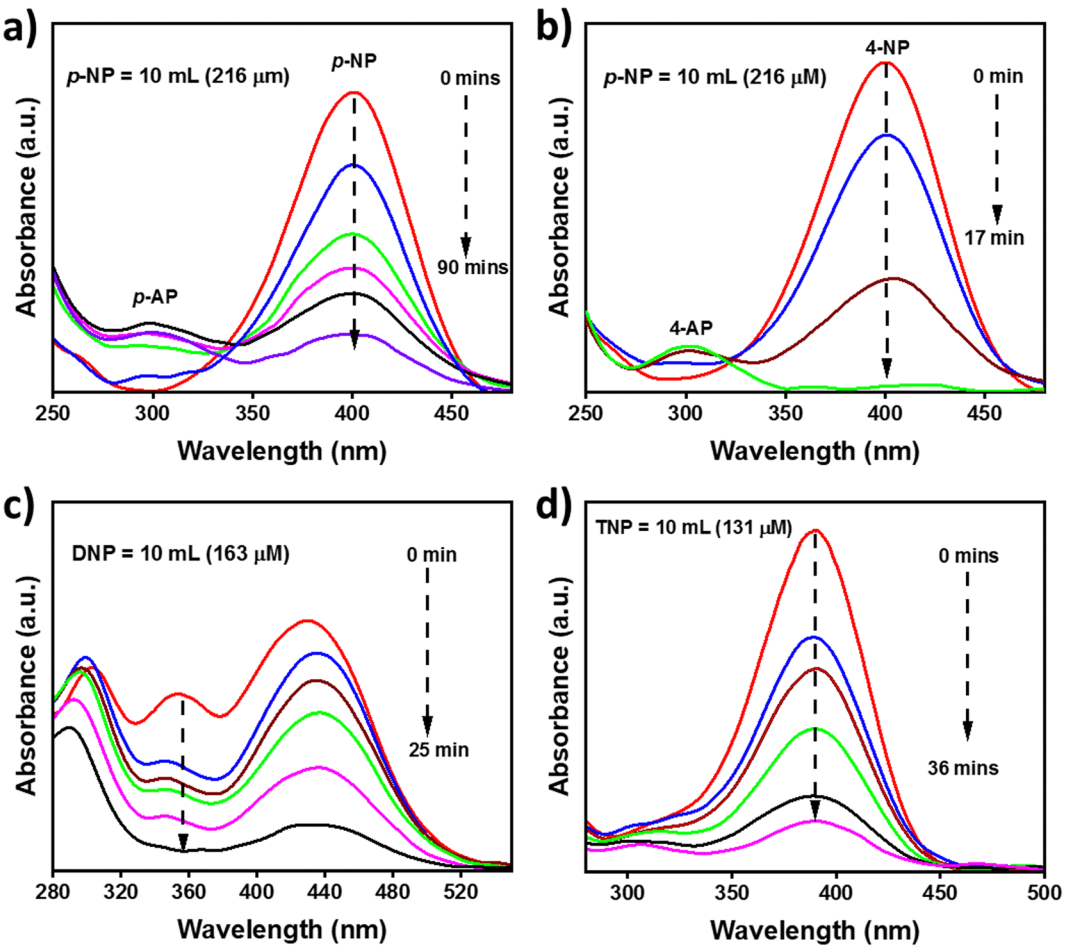

Fig. 9 UV-Vis absorption spectra revealing the reduction process of 10 mL of 4-nitrophenol (216 μM) with 1 mg of (a) Ta_2AlC and (b) Ta_2C. (c) The reduction process of 10 mL of 2,4-dinitrophenol (DNP) (163 μM) with 1 mg of Ta_2C and (d) 10 mL of 2,4,6-trinitrophenol (TNP) (131 μM) with 1 mg of Ta_2C.

Table 1 Comparison of the catalytic performance for 4-nitrophenol reduction

Material	Catalyst (mg mL^{-1})	Concentration of 4-NP (mM)	Volume of 4-NP (mL)	Time for completion of the reaction (min)	Ref.
$Cu_2O/TiO_2/Ti_3C_2$	0.3	5	2	40	52
CQD@Ag/MXene	0.0040	10	0.015	2	25
Cu/GDY	0.05	0.19	1	2.7	11
MXene@AgPd/PDA	0.06	0.1	50	1	53
Pd/CNT	1	1	4	30	54
Nb_4C_3@PdNPs	0.033	0.133	0.4	2.75	32
Zn/SnO_2	1.5	2	0.12	22	55
$PANI/Bi_2O_3$	1	0.2	1	15	56
MoS_2/Ti_3C_2	1	2	0.25	5	57
$Au/CaCO_3$	1	1	2	3	45
Ti_3C_2@PdNPs	1	5	1	8	58
AgPd@UiO-66-NH_2	1.5	5	1.5	7	9
$CoFe_2O_4/C$	0.05	0.1	2.95	2.5	12
$CuFe_2O_4$	5	0.1	2.5	2	50
Ta_2C-E MXene	0.2	0.216	5	8	This work

of excess $NaBH_4$. It is apparent that Ta_2C MXene shows excellent catalytic activity towards the reduction of 4-nitrophenol at very low concentrations of Ta_2C.

4. Conclusions

In this work, Ta_2C MXene was synthesized from Ta_2AlC using a fluorine-free synthesis method, and the prepared MXene was confirmed using various characterization techniques. It is recognized that due to their layered structure, MXenes display improved catalytic activities, and hence the prepared Mxene was tested for its electrocatalytic activity towards the HER and nitrophenol reduction. Furthermore, the catalytic activity towards the reduction of substituted nitrophenols in the presence of excess $NaBH_4$ was also investigated. Under standard HER conditions, the electrocatalyst Ta_2C-E MXene exhibited overpotentials of 223 mV to reach the 10 mA cm^{-2} current density (0.5 M H_2SO_4). Furthermore, the electrocatalytic reduction behavior of Ta_2C MXene towards the electrochemical reduction of 4-NP was investigated in 1 M KOH. Galvanostatic electrolysis was performed in a divided cell using Ta_2C-E modified carbon cloth as the cathode, and Pt as the anode separated by a Nafion membrane, and it showed 72% product conversion and 96% faradaic efficiency. The progress of the galvanostatic electrolysis was monitored using *ex situ* Raman and UV-Vis spectroscopy. Similarly, the reducing behavior of Ta_2C-E towards the reduction of 4-nitrophenol to 4-aminophenol in the presence of $NaBH_4$ was tested. Ta_2C-E MXene displayed improved catalytic activity with pseudo-first-order kinetics. To expand the scope of catalysis, substituted nitrophenols such as 2,4-dinitrophenol and 2,4,6-trinitrophenol were tested under similar conditions. Ta_2C nanoparticles completely reduced all three nitro compounds (10 mL each), 4-NP (216 μM), DNP (163 μM) and TNP (131 μM) in 17, 25 and 36 min, respectively. It is apparent that in all these studies, the Ta_2C MXene displayed improved catalytic performance and stability. This study indicates that MXene-based catalysts can be successfully applied in chemical catalysis as well as electrocatalysis. Furthermore, the scope of MXene catalysis can be improved by compositing these layered materials with transition metal ions which shows outstanding performance and stability in water splitting and nitrophenol conversion. Our method combines reticular chemistry with materials electrochemistry, and this method is helpful in the development of new catalysts for applications in organic synthesis and toxic chemical reduction.

Conflicts of interest

The authors declare no conflicts of interest.

Acknowledgements

The authors would like to acknowledge the Director of CSIR-CECRI, Karaikudi and staff members for their constant support and encouragement. Dr M. K. acknowledges CSIR-FIRST (MLP-1004) for financial support. CSIR-CECRI manuscript number: CECRI/PESVC/Pubs/2023-052.

References

1 X. Li, X. Lv, X. Sun, C. Yang, Y.-Z. Zheng, L. Yang, S. Li and X. Tao, *Appl. Catal., B*, 2021, **284**, 119708.
2 Y. Li, L. Ding, Y. Guo, Z. Liang, H. Cui and J. Tian, *ACS Appl. Mater. Interfaces*, 2019, **11**, 41440–41447.
3 W.-F. Chen, J. T. Muckerman and E. Fujita, *Chem. Commun.*, 2013, **49**, 8896–8909.
4 H. S. Gujral, M. Fawaz, S. Joseph, C. I. Sathish, G. Singh, X. Yu, M. B. H. Breese, J. Yi, M. Singh, V. Bansal, A. Karakoti and A. Vinu, *ACS Appl. Nano Mater.*, 2022, **5**, 12077–12086.
5 H. N. Sumedha, M. Shashank, S. R. Teixeira, B. M. Praveen and G. Nagaraju, *Sci. Rep.*, 2022, **12**, 10776.
6 Z. W. Seh, K. D. Fredrickson, B. Anasori, J. Kibsgaard, A. L. Strickler, M. R. Lukatskaya, Y. Gogotsi, T. F. Jaramillo and A. Vojvodic, *ACS Energy Lett.*, 2016, **1**, 589–594.
7 Z. Kang, M. A. Khan, Y. Gong, R. Javed, Y. Xu, D. Ye, H. Zhao and J. Zhang, *J. Mater. Chem. A*, 2021, **9**, 6089–6108.
8 S. Gopi, S. Perumal, E. M. Al Olayan, O. D. AlAmri, A. S. Aloufi, M. Kathiresan and K. Yun, *Chemosphere*, 2021, **267**, 129243.

9 S. A. Hira, M. Nallal and K. H. Park, *Sens. Actuators, B*, 2019, **298**, 126861.
10 Y. M. Hunge, A. A. Yadav, S.-W. Kang, H. Kim, A. Fujishima and C. Terashima, *J. Hazard. Mater.*, 2021, **419**, 126453.
11 S. Xie, Z. Xu, C. Yu, X. Yu, Z. Zhang and J. Li, *ChemistrySelect*, 2021, **6**, 13572–13576.
12 Y. Zhao, B. Cao, Z. Lin and X. Su, *Environ. Pollut.*, 2019, **254**, 112961.
13 K. Seku, B. R. Gangapuram, B. Pejjai, M. Hussain, S. S. Hussaini, N. Golla and K. K. Kadimpati, *Chem. Pap.*, 2019, **73**, 1695–1704.
14 K. Naseem, R. Begum, Z. H. Farooqi, W. Wu and A. Irfan, *Appl. Organomet. Chem.*, 2020, **34**, e5742.
15 R. T. Yunarti, I. D. Isa, L. C. C. Dimonti, A. A. Dwiatmoko, M. Ridwan and J.-M. Ha, *Nano-Struct. Nano-Objects*, 2021, **26**, 100719.
16 M. Naguib, M. Kurtoglu, V. Presser, J. Lu, J. Niu, M. Heon, L. Hultman, Y. Gogotsi and M. W. Barsoum, *Adv. Mater.*, 2011, **23**, 4248–4253.
17 S. Ponnada, M. S. Kiai, D. B. Gorle, R. S. C. Bose, V. Rajagopal, B. Saini, M. Kathiresan, A. Nowduri, R. Singhal, F. Marken, M. A. Kulandainathan, K. K. Nanda and R. K. Sharma, *Catal. Sci. Technol.*, 2022, **12**, 4413–4441.
18 Y. Gogotsi and B. Anasori, *ACS Nano*, 2019, **13**, 8491–8494.
19 M. U. Khan, L. Du, S. Fu, D. Wan, Y. Bao, Q. Feng, S. Grasso and C. Hu, *Coatings*, 2022, **12**, 516.
20 K. A. Papadopoulou, A. Chroneos, D. Parfitt and S.-R. G. Christopoulos, *J. Appl. Phys.*, 2020, **128**, 170902.
21 S.-Y. Pang, Y.-T. Wong, S. Yuan, Y. Liu, M.-K. Tsang, Z. Yang, H. Huang, W.-T. Wong and J. Hao, *J. Am. Chem. Soc.*, 2019, **141**, 9610–9616.
22 J. Haemers, R. Gusmão and Z. Sofer, *Small Methods*, 2020, **4**, 1900780.
23 A. Rafieerad, A. Amiri, G. L. Sequiera, W. Yan, Y. Chen, A. A. Polycarpou and S. Dhingra, *Adv. Funct. Mater.*, 2021, **31**, 2100015.
24 J. Liu, W. Peng, Y. Li, F. Zhang and X. Fan, *Trans. Tianjin Univ.*, 2020, **26**, 149–171.
25 Y. Chen, C. Yang, X. Huang, L. Li, N. Yu, H. Xie, Z. Zhu, Y. Yuan and L. Zhou, *RSC Adv.*, 2022, **12**, 4836–4842.
26 T. Li, L. Yao, Q. Liu, J. Gu, R. Luo, J. Li, X. Yan, W. Wang, P. Liu, B. Chen, W. Zhang, W. Abbas, R. Naz and D. Zhang, *Angew. Chem., Int. Ed.*, 2018, **57**, 6115–6119.
27 D. A. Kuznetsov, Z. Chen, P. V. Kumar, A. Tsoukalou, A. Kierzkowska, P. M. Abdala, O. V. Safonova, A. Fedorov and C. R. Müller, *J. Am. Chem. Soc.*, 2019, **141**, 17809–17816.
28 K. P. Akshay Kumar, O. Alduhaish and M. Pumera, *Electrochem. Commun.*, 2021, **125**, 106977.
29 M. Sanna, S. Ng, J. V. Vaghasiya and M. Pumera, *ACS Sustainable Chem. Eng.*, 2022, **10**, 2793–2801.
30 T. A. Le, Q. V. Bui, N. Q. Tran, Y. Cho, Y. Hong, Y. Kawazoe and H. Lee, *ACS Sustainable Chem. Eng.*, 2019, **7**, 16879–16888.
31 Y. Tang, C. Yang, Y. Xie, Y. Kang, W. Que, J. Henzie and Y. Yamauchi, *ACS Sustainable Chem. Eng.*, 2023, **11**, 168–176.
32 N. Shabana, A. M. Arjun and P. A. Rasheed, *New J. Chem.*, 2022, **46**, 13622–13628.
33 H. Zhao, X. Pang, Y. Huang, Y. Bai, J. Ding, H. Bai and W. Fan, *Chem. Commun.*, 2022, **58**, 13499–13502.
34 G. Li, L. Tan, Y. Zhang, B. Wu and L. Li, *Langmuir*, 2017, **33**, 9000–9006.
35 T. S. Mathis, K. Maleski, A. Goad, A. Sarycheva, M. Anayee, A. C. Foucher, K. Hantanasirisakul, C. E. Shuck, E. A. Stach and Y. Gogotsi, *ACS Nano*, 2021, **15**, 6420–6429.
36 M. Naguib, O. Mashtalir, J. Carle, V. Presser, J. Lu, L. Hultman, Y. Gogotsi and M. W. Barsoum, *ACS Nano*, 2012, **6**, 1322–1331.
37 H. Lin, Y. Wang, S. Gao, Y. Chen and J. Shi, *Adv. Mater.*, 2018, **30**, 1703284.
38 N. J. Lane, M. Naguib, V. Presser, G. Hug, L. Hultman and M. W. Barsoum, *J. Raman Spectrosc.*, 2012, **43**, 954–958.
39 R. Sukanya, S. Ramki and S.-M. Chen, *Microchim. Acta*, 2020, **187**, 342.
40 Z. Liu, H. Lin, M. Zhao, C. Dai, S. Zhang, W. Peng and Y. Chen, *Theranostics*, 2018, **8**, 1648–1664.
41 J. Liu, Z. Meng, J. Liu, X. Zhu, C. Wang and L. Yang, *Mod. Phys. Lett. B*, 2019, **33**, 1950209.
42 T. Wu, X. Pang, S. Zhao, S. Xu, Z. Liu, Y. Li and F. Huang, *Small Struct.*, 2022, **3**, 2100206.
43 D. S. Silvester, A. J. Wain, L. Aldous, C. Hardacre and R. G. Compton, *J. Electroanal. Chem.*, 2006, **596**, 131–140.
44 A. Serrà, R. Artal, M. Pozo, J. Garcia-Amorós and E. Gómez, *Catalysts*, 2020, **10**, 458.
45 Q. Ding, Z. Kang, L. Cao, M. Lin, H. Lin and D.-P. Yang, *Appl. Surf. Sci.*, 2020, **510**, 145526.
46 C. Wang, D. Zhu, H. Bi, Z. Zhang and J. Zhu, *Int. J. Mol. Sci.*, 2023, **24**, 2432.
47 S. Mourdikoudis, V. Montes-García, S. Rodal-Cedeira, N. Winckelmans, I. Pérez-Juste, H. Wu, S. Bals, J. Pérez-Juste and I. Pastoriza-Santos, *Dalton Trans.*, 2019, **48**, 3758–3767.
48 C. L. Jahncke, W. Zhang, B. M. DeMuynck and A. D. Hill, *J. Chem. Educ.*, 2022, **99**, 3233–3241.
49 F. Bao, F. Tan, W. Wang, X. Qiao and J. Chen, *RSC Adv.*, 2017, **7**, 14283–14289.
50 A. G. Ramu, S. Salla, S. Chandrasekaran, P. Silambarasan, S. Gopi, S.-Y. Seo, K. Yun and D. Choi, *Environ. Pollut.*, 2021, **270**, 116063.
51 K. Karakas, A. Celebioglu, M. Celebi, T. Uyar and M. Zahmakiran, *Appl. Catal., B*, 2017, **203**, 549–562.
52 J. Yin, B. Ge, T. Jiao, Z. Qin, M. Yu, L. Zhang, Q. Zhang and Q. Peng, *Langmuir*, 2021, **37**, 1267–1278.
53 J. Jin, S. Wu, J. Wang, Y. Xu, S. Xuan and Q. Fang, *Dalton Trans.*, 2023, **52**, 2335–2344.
54 J. Audevard, A. Benyounes, R. Castro Contreras, H. Abou Oualid, M. Kacimi and P. Serp, *ChemCatChem*, 2022, **14**, e202101783.
55 S. K. Jain, U. Farooq, F. Jamal, A. Kalam and T. Ahmad, *Mater. Today Proc.*, 2021, **36**, 717–723.
56 G. Joseph, D. Pinheiro, M. K. Mohan and S. Devi Kalathiparambil Rajendra Pai, *Polym. Bull.*, 2023, **80**, 8467–8481.
57 S. Yang, Q. Liu, X. Wan, J. Jiang and L. Ai, *J. Alloys Compd.*, 2022, **891**, 161900.
58 J. Yin, L. Zhang, T. Jiao, G. Zou, Z. Bai, Y. Chen, Q. Zhang, M. Xia and Q. Peng, *Nanomaterials*, 2019, **9**, 1009.